Plasma pressure effect on Alfvén cascade eigenmodes

B. N. Breizman and M. S. Pekker
Institute for Fusion Studies, The University of Texas, Austin, Texas 78712

S. E. Sharapov and JET EFDA contributors[a)]
Euratom/UKAEA Fusion Association, Culham Science Center, Abingdon, Oxfordshire OX14 3DB, United Kingdom

(Received 19 August 2005; accepted 7 October 2005; published online 28 November 2005)

Tokamak plasmas with reversed magnetic shear are prone to the excitation of Alfvén cascade (AC) eigenmodes by energetic particles. These modes exhibit a quasiperiodic pattern of predominantly upward frequency sweeping. Observations also reveal that the AC spectral lines sometimes bend at low frequencies, which is a significant deviation from the shear Alfvén wave dispersion relation. This paper shows that the underlying reasons for such bending are the finite pressure of the plasma and the geodesic curvature that precludes shear Alfvén perturbations from being strictly incompressible. In addition to the geodesic effect, there are two other pressure effects on shear Alfvén waves, which are the convection in the presence of an equilibrium pressure gradient and the toroidicity-induced coupling between shear Alfvén waves and acoustic modes. An analytical treatment of the problem enables a parametric comparison of all three mechanisms. The key distinction between the geodesic compressibility and the acoustic coupling is that geodesic compression occurs without plasma displacement along the magnetic-field lines. As a result, the mode phase velocity is greater than the ion thermal velocity even in an isothermal plasma, which allows the mode to avoid a strong ion Landau damping. Plasma temperature diagnostics via magnetohydrodynamic spectroscopy employing the low-frequency part of the ACs is suggested.
 [DOI: 10.1063/1.2130692]

I. INTRODUCTION

The term "Alfvén cascades" (ACs) was introduced in Refs. 1–4 for tagging a special set of Alfvén modes observed in experiments on the Joint European Torus (JET) tokamak with a nonmonotonic safety-factor profile and a population of energetic ions generated by ion cyclotron resonance frequency (ICRF) heating. These modes were first found in JT-60U and they are also known as reversed shear Alfvén eigenmodes.[5] Most recently, Alfvén cascades have received considerable attention in the Alcator C-Mod experiment.[6] ACs have also been observed in deuterium-tritium (DT) experiments on tokamak fusion test reactor (TFTR)[7] and in neutral beam injection (NBI) experiments on JET and DIII-D.[8]

Alfvén cascade modes are known to be associated with a minimum in the radial profile of the safety factor q. The AC frequency $\omega_{\mathrm{AC}}(t)$ usually tracks the local dispersion relation for shear Alfvén waves in low-pressure plasmas:

$$\omega_{\mathrm{AC}}(t) \approx \left| \frac{m}{q_0(t)} - n \right| \frac{V_A}{R}, \tag{1}$$

where n and m are the toroidal and poloidal mode numbers, respectively, R is the major radius, q_0 is the minimum value of the safety factor, and V_A is the Alfvén velocity at $q=q_0$. At large mode numbers, the time dependence of V_A is less important than that of q_0. The underlying reason is that $q_0^{-1}(t)$ is multiplied by a large number m, whereas the quantity $|mq_0^{-1}-n|$ in front of $V_A(t)$ does not exceed $1/2q_0$, the value at which the AC frequency reaches the toroidal Alfvén eigenmode (TAE) frequency. As the value of $q_0(t)$ changes during the discharge, the mode frequency changes at a rate

$$\frac{d}{dt}\omega_{\mathrm{AC}}(t) \approx m\frac{V_A}{R}\frac{d}{dt}q_0^{-1}(t), \tag{2}$$

which is an important distinctive feature of Alfvén cascades. The robust relation between the mode frequency and $q_0(t)$ makes ACs a very convenient diagnostic tool for measuring the temporal evolution of the safety factor.[9,10] This technique is routinely used in JET advanced scenarios to facilitate the creation of internal transport barriers.

In agreement with Eq. (2), the observed rate of frequency sweeping is faster for higher mode numbers. It is common that q_0 decreases in time, which makes the modes with $m>nq_0$ sweep upward in frequency and the modes with $m<nq_0$ sweep downward. The experiments usually exhibit upward rather than downward sweeping, giving a strong preference to modes with $m>nq_0$. This feature results from a specific linear response of energetic particles with large orbits.[2] For large mode numbers, a small decrease in q_0 from m/n to $q_{\mathrm{TAE}}\equiv(2m-1)/2n$ increases the frequency from zero to the characteristic TAE frequency, $\omega_{\mathrm{TAE}}\approx V_A/2q_{\mathrm{TAE}}R$. The quantity $1/q_0$ can be treated as a linear function of time over the small interval $\delta q_0=1/2n$. As a result, the mode frequency is also a linear function of time over most of the sweeping interval, as Fig. 1 shows.

[a)]See the Appendix of J. Pamela *et al.*, *Fusion Energy 2004*, Proceedings of the 20th International Conference on Fusion Energy, Vilamoura, 2004, (IAEA, Vienna, 2004).

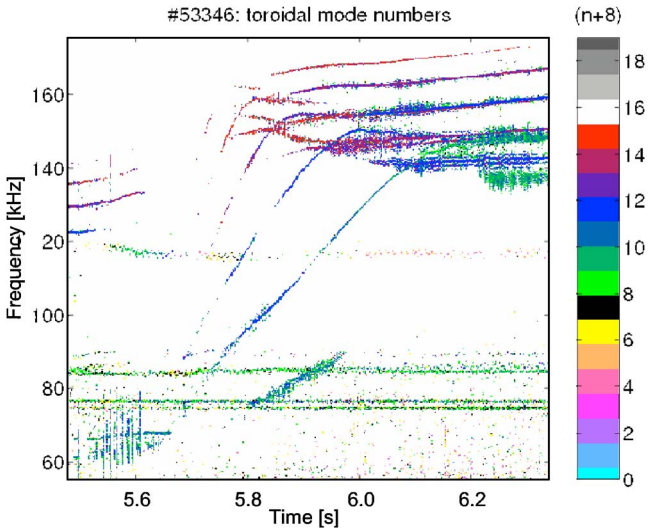

FIG. 1. (Color online). Magnetic spectrogram showing spectral lines of ACs and TAEs in typical JET discharge (pulse No. 53346). Different colors correspond to modes with different toroidal mode numbers. It is seen that ACs with different toroidal mode numbers terminate at different lowest frequencies due to the continuum damping effect.

When the value of q_0 is not too close to q_{TAE}, each AC mode consists of predominantly one poloidal Fourier component. However, as q_0 approaches q_{TAE}, toroidicity-induced coupling changes the mode structure to a sum of two comparable harmonics (m and $m-1$). Toroidal coupling also modifies the dispersion relation (1) near the TAE gap. This transition is seen as spectral line bending in Fig. 1 near the TAE gap. The corresponding theory has been developed in Ref. 4.

Another significant modification of Eq. (1) occurs at low frequencies (when q_0 is close to m/n). Observations reveal that the cascade modes never reach zero frequency at $q_0 = m/n$, as one would expect from Eq. (1). The spectral lines either terminate at low frequencies as seen in Fig. 1 or they become bowl shaped around a common minimum frequency for several modes as seen in Fig. 2. Continuum damping together with other damping mechanisms can readily account for the mode suppression,[11] but not for the spectral line bending. The latter requires a different underlying mechanism.

Unlike in the TAE frequency range, toroidal coupling between shear Alfvén waves is insignificant at low frequencies. Instead, pressure perturbation becomes the key factor. Toroidal geometry precludes shear Alfvén perturbations from being strictly incompressible. It produces a geodesic pressure perturbation given by

$$\delta P_G = -\gamma P_0 \,\mathrm{div}\left(\frac{\mathbf{B}_0}{B_0^2}\times\nabla\Phi\right) = -\gamma P_0\left(\nabla\Phi\cdot\mathrm{curl}\,\frac{\mathbf{B}_0}{B_0^2}\right), \tag{3}$$

where $c\,\partial\Phi/\partial t$ is the electrostatic potential associated with a shear Alfvén perturbation, γ is the effective ratio of specific heats (resulting from kinetic calculations), P_0 and $\mathbf{B}_0$ are the unperturbed pressure and magnetic field, respectively, and c is the speed of light. The impact of this geodesic perturbation on Alfvén cascades is the main subject of this paper. This

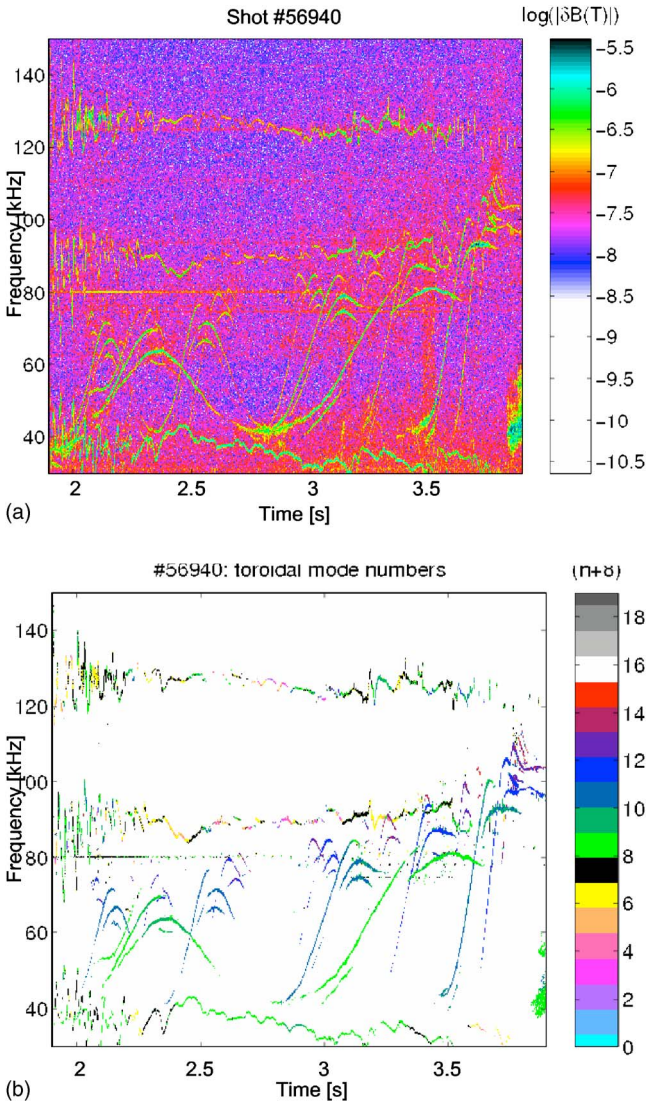

FIG. 2. (Color online). (a) Magnetic spectrogram showing the amplitude of the perturbed magnetic field due to ACs in JET discharge No. 56940. It is seen that ACs with different toroidal mode numbers reach the same lowest AC frequency. In contrast to Fig. 1, amplitudes of the ACs increase at low frequency, indicating lower damping rates. (b) Magnetic spectrogram showing toroidal mode numbers of ACs in (a).

effect is closely related to so-called geodesic acoustic modes.[12]

A significant modification of the Alfvén continuum due to plasma pressure was found numerically in Ref. 13 long before the discovery of Alfvén cascades. This finding is apparently relevant to what is seen in Fig. 2 because the cascade frequency tends to be close to the continuum, except when the mode reaches the TAE gap. However, Ref. 13 does not reveal the precise physics reason for the strong pressure effect on the Alfvén continuum. Given that, we opt to treat the problem analytically, which enables us to compare the underlying mechanisms and to identify the dominant one.

In addition to the geodesic effect, there are two other causes for plasma pressure perturbations in shear Alfvén waves. The first is convection. The perturbed pressure then arises from an incompressible displacement along the equilibrium pressure gradient, so that

$$\delta P_C = -\frac{1}{B_0^2}\nabla P_0 \cdot (\mathbf{B}_0 \times \nabla\Phi). \tag{4}$$

The second cause is the toroidicity-induced coupling between shear Alfvén waves and acoustic modes that causes a perturbed pressure

$$\delta P_A = -\gamma P_0\left(\mathbf{B}_0 \cdot \nabla\frac{\xi}{B_0}\right), \tag{5}$$

where ξ is the plasma displacement (along $\mathbf{B}_0$) in the acoustic perturbations. The coupling between shear Alfvén and acoustic modes occurs when the local shear Alfvén frequency (1) matches the local acoustic frequency for a neighboring poloidal mode number,

$$\omega = \frac{V_A}{R_0}\left|n - \frac{m}{q_0}\right| = \frac{C_s}{R_0}\left|n - \frac{m \pm 1}{q_0}\right|. \tag{6}$$

In low-beta plasma, the coupling condition requires q_0 to be very close to m/n, which immediately determines the corresponding value of the mode frequency:

$$\omega = \frac{C_S}{q_0 R_0}. \tag{7}$$

It is noteworthy that the geodesic effect can be clearly separated from the other two mechanisms in both its technical description and its physics consequences. In contrast to the convective mechanism, the geodesic effect involves plasma compression, and the resulting characteristic frequency scales as $\beta^{1/2}$, rather than β, with plasma pressure, which makes the convective mechanism insignificant at sufficiently low pressure. Ironically, plasma compressibility can be difficult to treat in magnetohydrodynamic (MHD) codes, which recently led to an artificial exclusion of this effect from the simulations of cascade modes in low-beta plasma in favor of a less relevant but more convenient convective effect.[14]

The key distinction between the geodesic compressibility and the acoustic coupling is that geodesic compression occurs without plasma displacement along the magnetic-field lines, and the corresponding characteristic frequency is $q_0\sqrt{2}$ times greater than that given by Eq. (7). As a result, the mode phase velocity is greater than the ion thermal velocity even in an isothermal plasma, which allows the mode to avoid a strong ion Landau damping.

It will be shown in this paper that all the pressure effects discussed above, together with the hot-ion effects,[2] modify the expression (1) for the Alfvén cascades as follows:

$$\omega_{\mathrm{AC}}(t) = \left[\left(\frac{m}{q_0(t)} - n\right)^2 \frac{V_A^2}{R_0^2} + \frac{2T_e}{M_i R_0^2}\left(1 + \frac{7}{4}\frac{T_i}{T_e}\right)\right]^{1/2} + \delta\omega, \tag{8}$$

where T_e and T_i are electron and ion temperatures, M_i is the ion mass, and the numerical coefficient 7/4 arises from kinetic calculations of specific heat ratios for electrons and ions (see, e.g., Ref. 15 and the more recent Ref. 16 discussing in detail the kinetic theory of low-frequency Alfvén modes in tokamaks). The temperature-dependent term in Eq. (8) describes the deformation of Alfvén continuum produced by plasma pressure. This deformation is most pronounced at low frequencies when q_0 is close to m/n so that the term $2T_e/(M_i R_0^2)[1+(7/4)(T_i/T_e)]$ can compete with the magnetic term $[m/q_0(t)-n]^2 V_A^2/R_0^2$ in a low-beta plasma. The quantity $\delta\omega$ determines a small deviation of the AC eigenfrequency from the deformed continuum due to effects of toroidal geometry,[4] hot ions,[2] and plasma pressure gradient.

II. BASIC EQUATIONS

We start with a linear ideal MHD description. Let $\delta\mathbf{r}$ be the displacement of a plasma element from its equilibrium position. We then have the following set of equations for the displacement $\delta\mathbf{r}$, the perturbed pressure δP, and the perturbed magnetic field $\delta\mathbf{B}$ (see, e.g., Ref. 17):

$$\rho_0\frac{\partial^2\delta\mathbf{r}}{\partial t^2} = -\nabla\delta P - \frac{1}{4\pi}\nabla(\mathbf{B}_0\cdot\delta\mathbf{B}) + \frac{1}{4\pi}(\mathbf{B}_0\cdot\nabla)\delta\mathbf{B} + \frac{1}{4\pi}(\delta\mathbf{B}\cdot\nabla)\mathbf{B}_0, \tag{9}$$

$$\delta P = -\delta\mathbf{r}\cdot\nabla P_0 - \gamma P_0 \,\mathrm{div}\,\delta\mathbf{r}, \tag{10}$$

$$\delta\mathbf{B} = \mathrm{curl}(\delta\mathbf{r}\times\mathbf{B}_0). \tag{11}$$

The quantities ρ_0, P_0, and $\mathbf{B}_0$ are the unperturbed density, pressure, and magnetic field, respectively. The unperturbed pressure and magnetic field satisfy the condition of plasma equilibrium,

$$0 = -\nabla\left(P_0 + \frac{1}{8\pi}B_0^2\right) + \frac{1}{4\pi}(\mathbf{B}_0\cdot\nabla)\mathbf{B}_0. \tag{12}$$

We employ the following representation for plasma displacement:

$$\delta\mathbf{r} = \xi\frac{\mathbf{B}_0}{B_0} + \frac{1}{B_0^2}(\mathbf{B}_0\times\nabla\Phi) + \frac{1}{B_0}\nabla\Psi - \frac{1}{B_0^3}\mathbf{B}_0(\mathbf{B}_0\cdot\nabla\Psi), \tag{13}$$

where the functions ξ, Φ, and Ψ are associated with the three types of weakly coupled linear perturbations in low-pressure large-aspect-ratio plasma (ξ refers to acoustic perturbations, Φ to shear Alfvén perturbations, and Ψ to compressional Alfvén perturbations).

In order to derive a set of coupled equations for ξ, Φ, and Ψ we take three independent "projections" of Eq. (9) as follows:

$$\frac{\mathbf{B}_0}{B_0}\cdot\frac{\partial^2\delta\mathbf{r}}{\partial t^2} = -\frac{\mathbf{B}_0}{\rho_0 B_0}\cdot\nabla\left[\delta P + \frac{(\mathbf{B}_0\cdot\delta\mathbf{B})}{4\pi}\right] + \frac{1}{4\pi\rho_0}\frac{\mathbf{B}_0}{B_0}\cdot(\mathbf{B}_0\cdot\nabla)\delta\mathbf{B} + \frac{1}{4\pi\rho_0}\frac{\mathbf{B}_0}{B_0}\cdot(\delta\mathbf{B}\cdot\nabla)\mathbf{B}_0, \tag{14}$$

$$\mathrm{div}\,\frac{4\pi\rho_0}{B_0^2}\left(\mathbf{B}_0\times\frac{\partial^2\delta\mathbf{r}}{\partial t^2}\right)=-\,\mathrm{div}\left\{\frac{\mathbf{B}_0}{B_0^2}\times\nabla[4\pi\delta P+(\mathbf{B}_0\cdot\delta\mathbf{B})]\right\}+\mathrm{div}\left[\frac{\mathbf{B}_0}{B_0^2}\times(\mathbf{B}_0\cdot\nabla)\delta\mathbf{B}\right]+\mathrm{div}\left[\frac{\mathbf{B}_0}{B_0^2}\times(\delta\mathbf{B}\cdot\nabla)\mathbf{B}_0\right], \tag{15}$$

$$\mathrm{div}\,\frac{4\pi\rho_0}{B_0}\frac{\partial^2\delta\mathbf{r}_\perp}{\partial t^2}=-\,\mathrm{div}\,\frac{4\pi}{B_0}\nabla_\perp\left[\delta P+\frac{(\mathbf{B}_0\cdot\delta\mathbf{B})}{4\pi}\right]+\mathrm{div}\left[\frac{(\mathbf{B}_0\cdot\nabla)\delta\mathbf{B}}{B_0}\right]_\perp+\mathrm{div}\left[\frac{(\delta\mathbf{B}\cdot\nabla)\mathbf{B}_0}{B_0}\right]_\perp, \tag{16}$$

where subscript $\perp$ marks transverse components of a vector with respect to the unperturbed magnetic field $\mathbf{B}_0$.

In what follows we reduce Eqs. (14)–(16) to a single equation for the shear Alfvén variable Φ in the limit of large n and m. This reduction involves two small dimensionless parameters: $\beta\equiv 4\pi P_0/B_0^2\ll 1$ and $\varepsilon\equiv a/R\ll 1$, where a is the minor radius and R is the major radius of the plasma torus. We will consider mode frequencies ω in the range of C_S/R, where C_S is the sound speed. These frequencies are much lower than the characteristic frequency of compressional Alfvén perturbations. The latter scales as mV_A/a, where V_A is the Alfvén speed. To perform a rough preliminary ordering, we assume that the characteristic scale lengths for ξ, Φ, and Ψ in the radial and toroidal directions are a/m and R/n, respectively. We also assume that the value of β meets the following constraint:

$$\varepsilon^2/m\ll\beta\ll\varepsilon, \tag{17}$$

which is consistent with typical experimental conditions.

A. Compressional Alfvén mode equation

We note that the inertial term and the δP term in Eq. (16) can be estimated as

$$\mathrm{div}\,\frac{4\pi\rho_0}{B_0}\frac{\partial^2\delta\mathbf{r}_\perp}{\partial t^2}\approx\frac{4\pi\rho_0}{B_0}\frac{m}{a}\omega^2|\delta\mathbf{r}_\perp|\approx\frac{4\pi P_0}{B_0}\frac{m\varepsilon^2}{a^3}|\delta\mathbf{r}_\perp|, \tag{18}$$

$$\mathrm{div}\,\frac{4\pi}{B_0}\nabla_\perp\delta P\approx\frac{4\pi P_0}{B_0}\frac{m^3}{a^3}|\delta\mathbf{r}_\perp|, \tag{19}$$

where we only consider the part of the δP term, associated with the cross-field displacement of the plasma. These estimates show that the inertial term can be safely neglected in Eq. (16) compared with the δP term. The two line-bending terms in Eq. (16) are also much smaller than the δP term, provided that β is much greater than ε^2/m, which we consider to be the case here. It is then allowable to replace Eq. (16) by the condition of the balance between the perturbed pressure of the thermal plasma and the perturbed magnetic-field pressure,

$$4\pi\delta P+(\mathbf{B}_0\cdot\delta\mathbf{B})=0. \tag{20}$$

This condition can be rewritten in terms of ξ, Φ, and Ψ with only the dominant terms retained:

$$4\pi\gamma P_0(\mathbf{B}_0\cdot\nabla)\frac{\xi}{B_0}+4\pi\gamma P_0\,\mathrm{div}\left(\frac{\mathbf{B}_0}{B_0^2}\times\nabla\Phi\right)+\frac{4\pi}{B_0^2}\nabla\Phi\cdot(\nabla P_0\times\mathbf{B}_0)+\mathrm{div}(B_0\nabla\Psi)=0. \tag{21}$$

B. Acoustic-mode equation

Substitution of Eqs. (10), (11), and (13) into Eq. (14) gives the following acoustic-mode equation in terms of ξ, Φ, and Ψ:

$$\frac{\partial^2}{\partial t^2}\frac{\xi}{B_0}-\frac{\gamma P_0}{\rho_0}\left(\frac{\mathbf{B}_0}{B_0}\cdot\nabla\right)\left(\frac{\mathbf{B}_0}{B_0}\cdot\nabla\right)\frac{\xi}{B_0}=\frac{\gamma P_0}{\rho_0}\frac{\mathbf{B}_0}{B_0^2}\cdot\nabla\left(\nabla\Phi\cdot\mathrm{curl}\,\frac{\mathbf{B}_0}{B_0^2}\right)+\frac{\gamma P_0}{\rho_0}\frac{\mathbf{B}_0}{B_0^2}\cdot\nabla\left(\mathrm{div}\,\frac{\nabla\Psi}{B_0}\right)-\frac{\gamma P_0}{\rho_0}\frac{\mathbf{B}_0}{B_0^2}\cdot\nabla\left[\mathrm{div}(\mathbf{B}_0\cdot\nabla\Psi)\frac{\mathbf{B}_0}{B_0^3}\right]. \tag{22}$$

This equation simplifies to

$$\frac{\partial^2}{\partial t^2}\frac{\xi}{B_0}-\frac{\gamma P_0}{\rho_0}\left(\frac{\mathbf{B}_0}{B_0}\cdot\nabla\right)\left(\frac{\mathbf{B}_0}{B_0}\cdot\nabla\right)\frac{\xi}{B_0}=\frac{\gamma P_0}{\rho_0}\frac{\mathbf{B}_0}{B_0^2}\cdot\nabla\left(\nabla\Phi\cdot\mathrm{curl}\,\frac{\mathbf{B}_0}{B_0^2}\right) \tag{23}$$

if one neglects the Ψ terms in accordance with the estimate for such terms from (21).

C. Shear Alfvén mode equation

The transformation of the shear Alfvén mode equation, Eq. (15), goes as follows: we neglect the Ψ contribution to the inertial term, omit the compressional term on the right-hand side in accordance with Eq. (20), and use a reduced expression for $\delta\mathbf{B}$ in the line-bending terms on the right-hand side:

$$\delta\mathbf{B}=-\,\mathrm{curl}\left[\mathbf{B}_0\left(\frac{\mathbf{B}_0}{B_0^2}\cdot\nabla\Phi\right)\right]-\frac{\mathbf{B}_0}{B_0^2}\,\mathrm{div}(B_0\nabla\Psi). \tag{24}$$

We then obtain

$$-\operatorname{div}\frac{4\pi\rho_0}{B_0^2}\nabla_\perp\frac{\partial^2\Phi}{\partial t^2}=-2\left[\frac{\mathbf{B}_0}{B_0^2}\times\left(\frac{\mathbf{B}_0}{B_0}\cdot\nabla\right)\frac{\mathbf{B}_0}{B_0}\right]\cdot\nabla\operatorname{div}(B_0\nabla\Psi)-\operatorname{div}\left\{\frac{\mathbf{B}_0}{B_0^2}\times(\mathbf{B}_0\cdot\nabla)\operatorname{curl}\left[\left(\frac{\mathbf{B}_0}{B_0^2}\cdot\nabla\Phi\right)\mathbf{B}_0\right]\right\}$$
$$-\operatorname{div}\left(\frac{\mathbf{B}_0}{B_0^2}\times\left\{\operatorname{curl}\left[\left(\frac{\mathbf{B}_0}{B_0^2}\cdot\nabla\Phi\right)\mathbf{B}_0\right]\cdot\nabla\right\}\mathbf{B}_0\right). \tag{25}$$

For high mode numbers, this equation can be further transformed to

$$\operatorname{div}\frac{4\pi\rho_0}{B_0^2}\nabla_\perp\frac{\partial^2\Phi}{\partial t^2}=\operatorname{div}\left(\frac{\mathbf{B}_0}{B_0}\cdot\nabla\right)\left(\frac{\mathbf{B}_0}{B_0}\cdot\nabla\right)\nabla_\perp\Phi-8\pi\gamma\left[\frac{\mathbf{B}_0}{B_0^2}\times\left(\frac{\mathbf{B}_0}{B_0}\cdot\nabla\right)\frac{\mathbf{B}_0}{B_0}\right]\cdot\nabla\left[P_0\operatorname{div}\left(\frac{\mathbf{B}_0}{B_0^2}\times\nabla\Phi\right)\right]-8\pi\left[\frac{\mathbf{B}_0}{B_0^2}\right.$$
$$\left.\times\left(\frac{\mathbf{B}_0}{B_0}\cdot\nabla\right)\frac{\mathbf{B}_0}{B_0}\right]\cdot\nabla\left[\frac{1}{B_0^2}\nabla\Phi\cdot(\nabla P_0\times\mathbf{B}_0)\right]-8\pi\gamma\left[\frac{\mathbf{B}_0}{B_0^2}\times\left(\frac{\mathbf{B}_0}{B_0}\cdot\nabla\right)\frac{\mathbf{B}_0}{B_0}\right]\cdot\nabla\left[P_0(\mathbf{B}_0\cdot\nabla)\frac{\xi}{B_0}\right], \tag{26}$$

where Eq. (21) was used to eliminate the Ψ contribution.

Equations (23) and (26) form a closed set of coupled equations for acoustic and shear Alfvén waves.

III. DEFORMATION OF ALFVÉN CONTINUUM AND ALFVÉN CASCADES

It follows from a straightforward analysis that the coupling term in Eq. (26) is actually smaller (by a factor $2q_0^2\gg 1$) than the second term on the right-hand side of that equation. As a result, the phase velocity of the shear Alfvén mode remains supersonic even at lowest frequencies. We therefore neglect the contribution associated with ξ to Eq. (26). We also neglect the convective term with ∇P_0 for a better illustration of the geodesic deformation effect alone. The ∇P_0 contribution to the eigenmode equation will then be evaluated separately. We thus obtain

$$\operatorname{div}\frac{4\pi\rho_0}{B_0^2}\nabla_\perp\frac{\partial^2\Phi}{\partial t^2}=\operatorname{div}\left(\frac{\mathbf{B}_0}{B_0}\cdot\nabla\right)\left(\frac{\mathbf{B}_0}{B_0}\cdot\nabla\right)\nabla_\perp\Phi-8\pi\gamma\left[\frac{\mathbf{B}_0}{B_0^2}\times\left(\frac{\mathbf{B}_0}{B_0}\cdot\nabla\right)\frac{\mathbf{B}_0}{B_0}\right]\cdot\nabla\left[P_0\operatorname{div}\left(\frac{\mathbf{B}_0}{B_0^2}\times\nabla\Phi\right)\right]. \tag{27}$$

For our subsequent analysis of Eq. (27), we choose straight-field-line coordinates with the following representation for the unperturbed magnetic field:

$$\mathbf{B}_0=B_*\frac{r}{q(r)}\nabla r\times\nabla(q\theta-\varsigma), \tag{28}$$

where ς and θ are the toroidal and poloidal angles, respectively, r is the flux coordinate, $q(r)$ is the safety factor, and B_* is the value of the unperturbed field on the magnetic axis. The function Φ, which is a periodic function of ς and θ, can be represented by a Fourier series as follows:

$$\Phi(r;\theta;\varsigma;t)=\exp(in\varsigma-i\omega t)\sum_m\Phi_m(r)\exp(-im\theta)+\text{c.c.}, \tag{29}$$

where ω is the mode frequency and $\Phi_m(r)$ is the radial structure for the m-th poloidal harmonic.

Similar to the procedure described in Ref. 4, Eq. (27) can be written as a set of coupled equations for $\Phi_j(r)$:

$$\hat{L}_{l;j}\Phi_j(r)=0, \tag{30}$$

where the operators $\hat{L}_{l;j}$ are given in the Appendix and the summation over j is implied with j running from $m-1$ through $m+1$ for a mode with the m-th dominant poloidal harmonic. Such a truncation includes all the essential effects determined by the main and two satellite harmonics arising from the toroidal coupling effect, but it neglects $m\pm 2$ contributions that are small at low β.

Furthermore, the procedure of Ref. 4 transforms Eq. (27) into an eigenmode equation for Φ_m:

$$\frac{\partial}{\partial r}\left[\frac{\omega^2}{V_A^2}-\frac{1}{R_0^2}\left(n-\frac{m}{q}\right)^2-\frac{2C_S^2}{V_A^2R_0^2}\right]r\frac{\partial\Phi_m}{\partial r}$$
$$-\frac{m^2}{r}\left[\frac{\omega^2}{V_A^2}-\frac{1}{R_0^2}\left(n-\frac{m}{q}\right)^2-\frac{2C_S^2}{V_A^2R_0^2}\right]\Phi_m$$
$$=\frac{m^2}{r}\frac{\omega^2}{V_A^2}\left[2\frac{\varepsilon^2+2\varepsilon\Delta'}{(2qn-2m)^2-1}\right]\Phi_m, \tag{31}$$

where the neglected terms contain either an additional small factor $(1/m)\ll 1$ or an additional inverse aspect ratio factor ε with respect to the retained $O(\varepsilon^2)$ terms. In order to investigate AC characteristics at their lowest frequency, we delineate the effects associated with the low-frequency deformation of the Alfvén continuum [left-hand side of Eq. (31)] from the effects that give a deviation $\delta\omega$ of the eigenmode frequency from the Alfvén continuum [right-hand side of Eq. (31)].

A. Low-frequency deformation of Alfvén continuum

The dispersion relation for the Alfvén continuum is determined by a vanishing multiplier in front of the second-order derivative in Eq. (31), which gives

$$\Omega^2 - 4(m-nq)^2 - 8q^2\frac{C_S^2}{V_A^2} = 0 \tag{32}$$

for the normalized frequency

$$\Omega = \frac{2\omega q R_0}{V_A}. \tag{33}$$

Here, the ion-sound speed $C_S^2=[T_e+(7/4)T_i]/M_i$ involves specific heats of electrons and ions calculated from the kinetic theory in toroidal geometry.[15] Thus one sees that the low-frequency region of the dispersion relation, Eq. (32), is sensitive to the value of T_e/T_i.

The last term in Eq. (32) describes the geodesic deformation of the Alfvén continuum, and it determines the lowest frequency of an Alfvén cascade with mode numbers n and m achieved when the minimum value of the safety factor q_0 satisfies $m-nq_0=0$:

$$\Omega^2_{\text{Geodesic}} = 8q_0^2\frac{C_S^2}{V_A^2}. \tag{34}$$

This expression for the minimum frequency is insensitive to the mode number in agreement with experimental data for ACs.[1–6]

The additional deformation of Alfvén continuum due to the toroidal coupling to the acoustic wave described by two coupled equations [(23) and (26)] rather than simplified single equation (27) modifies the last term in Eq. (32) to

$$-8q_0^2\frac{C_S^2}{V_A^2}\left[1 - \frac{2(C_S/V_A)^2(nq_0-m-1)^2}{-\Omega^2+4(C_S/V_A)^2(nq_0-m-1)^2} - \frac{2(C_S/V_A)^2(nq_0-m+1)^2}{-\Omega^2+4(C_S/V_A)^2(nq_0-m+1)^2}\right]. \tag{35}$$

The corresponding modified solution of Eq. (32) at the rational surface is

$$\Omega^2 = 8q_0^2\frac{C_S^2}{V_A^2}\left(1+\frac{1}{2q_0^2}\right). \tag{36}$$

This expression, together with Eq. (34), shows that the acoustic deformation of the Alfvén continuum is indeed weaker than the geodesic deformation for typically high values of the safety factor in the shear-reversed tokamak plasmas,

$$2q_0^2 \gg 1. \tag{37}$$

B. Eigenmode equation

The deviation $\delta\omega$ of the AC eigenfrequency from the Alfvén continuum is determined by the right-hand side of the eigenmode equation (31). This equation can be analyzed similarly to Refs. 2 and 4 by expanding the parallel wavenumber parameter about the point of zero magnetic shear $r=r_0$, where $q(r_0)\equiv q_0$ is the minimum value of the safety factor:

$$\frac{1}{R_0^2}\left[n-\frac{m}{q(r)}\right]^2 \cong \frac{1}{R_0^2}\left(n-\frac{m}{q_0}\right)^2 + \frac{mq''(r)}{q_0^2}\frac{(r-r_0)^2}{R_0^2}\left(n-\frac{m}{q_0}\right), \tag{38}$$

so that the eigenmode equation is simplified to

$$\frac{d}{dx}(S+x^2)\frac{d}{dx}\Phi_m - \left[S+x^2-Q\frac{\Omega_0}{2(m-nq_0)}\right]\Phi_m = 0, \tag{39}$$

where $x=m(r-r_0)/r_0$ is the dimensionless radial variable and $\delta\omega$ is characterized by the parameter

$$S = \frac{m}{4(m-nq_0)}\frac{q_0}{r_0^2 q_0''}\times\left[\Omega^2 - 4(m-nq_0)^2 - 8q_0^2\frac{C_S^2}{V_A^2}\right]. \tag{40}$$

Same as in Refs. 2–4, the quantity Q provides a potential well for the existence of a discrete eigenmode. Equation (31) gives

$$Q = Q_{\text{tor}} = m\frac{\Omega_0^2}{2(m-nq_0)}\frac{q_0}{r_0 q_0''}\frac{\varepsilon_0(\varepsilon_0+2\Delta_0')}{[1-(2q_0n-2m)^2]}, \tag{41}$$

where Ω_0^2 is given by Eq. (32) with the value of the safety factor taken at the zero shear point $q=q_0$.

The analysis of Eq. (39) can be performed similar to those in Refs. 2–4 to obtain the following dispersion relation:

$$S = Q^* - (2l+1)\sqrt{Q^*}, \quad Q^* \gg 1, \qquad S = C\exp\left(-\frac{2\pi}{\sqrt{Q^*-1/4}}\right), \quad Q^* - 1/4 \ll 1, \tag{42}$$

where $Q^*\equiv Q\Omega_0/2(m-nq_0)$ and $C\approx 43.2$ is a constant.[18]

In the presence of a significant population of energetic ions with orbit width exceeding the radial size of the mode, and with thermal plasma pressure gradient taken into account, the value of Q consists of three contributions: the contribution due to the toroidicity Q_{tor}, due to the hot ions Q_{hot}, and due to the thermal plasma pressure gradient Q_{pressure}:

$$Q = Q_{\text{tor}} + Q_{\text{hot}} + Q_{\text{pressure}}, \tag{43}$$

where the contribution from the hot ions was calculated in Ref. 2

$$Q_{\text{hot}} = \omega_0^2\frac{q_0^2R_0^2}{V_A^2(m-nq_0)}\frac{q_0}{r_0^2q_0''}\left[\left(-\frac{r}{\rho}\frac{d\langle\rho_h\rangle}{dr}\right)_{r=r_0}\frac{\omega_{\text{ch}}}{\omega_0}\right]. \tag{44}$$

The fast-ion effect was found to facilitate the eigenmode formation in Ref. 2. The effect of the thermal plasma pressure gradient, on the contrary, plays a negative role in the mode formation. This can be seen from considering the case of $q_0=m/n$, so that the operators $\hat{L}_{i,j}$ from the Appendix take a simplified form, and using the approximation $(r\Delta')'-2\Delta'=0$ as in Ref. 4, one obtains

$$Q_{\text{pressure}} = -\frac{\alpha^2}{2(\Omega^2/4-1)}, \tag{45}$$

where

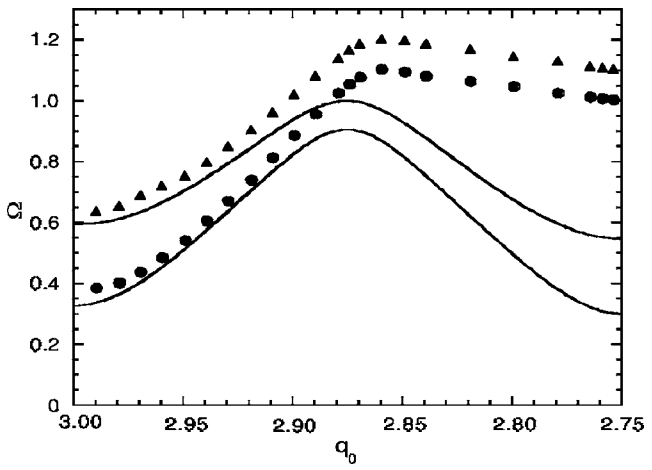

FIG. 3. Computed behavior of AC spectral lines showing the effect of plasma pressure on AC frequency (in units of the central TAE gap frequency) for the $n=3$ and $m=11,12$ eigenmodes as a function of safety factor q_0. Solid curve represents the MHD continuum, and the triangular and circular points are for the values of β of 0.005 and 0.0015, respectively.

$$\alpha = -\frac{8\pi q_0^2 R_0}{B_0^2}\frac{dP_0}{dr}. \tag{46}$$

It is seen from Eq. (45) that the pressure gradient term for ACs with frequencies below the TAE gap always has the sign corresponding to a potential "hill," not to a potential "well" for the ACs. This conclusion is opposite to the one made for the pressure gradient effect on ACs in Ref. 14 because of the wrong signs in Eqs. (9) and (10) of Ref. 14. Thus the interpretation suggested in Ref. 14 for the ACs obtained with the NOVA-K code is inconsistent, and an alternative effect should be sought.

In applying our theory to JET experiments, we note that q_0 typically varies from 4 to 2 in the shear-reversed discharges, so that $1/2q_0^2$ is indeed small in such experiments. Substituting typical values of the safety factor and plasma pressure into a code developed for calculations of the pressure effect on ACs in toroidal geometry, one sees from Fig. 3 that the minimum frequencies are an appreciable fraction of the TAE frequency for a quite low beta. This geodesic limitation on the Alfvén continuum frequency is independent of mode numbers n and m, and it appears to be the dominant reason for the experimental pattern seen in Fig. 2.

IV. PROSPECTIVE DIAGNOSTICS APPLICATIONS

Experimental data on Alfvén cascades is successfully used for diagnosing the time evolution of the minimum value of the safety factor $q_0(t)$ for facilitating the development of internal transport barriers in shear-reversed plasmas.[9,10] The evolution of $q_0(t)$ is derived from Eq. (2) and the clustering of ACs with different toroidal mode numbers in time.[1]

It is likely that additional information about plasma parameters can be obtained in view of the developed understanding of the low-frequency properties of ACs. Here, we point out first a possibility for diagnosing electron temperature T_e and/or the ratio of ion and electron temperatures, T_i/T_e, from observations of the lowest frequency of ACs. Such independent measurements are especially important for the early phase of plasma discharges. At the early phase the current-drive techniques, such as lower-hybrid current drive on JET, create a significant suprathermal population of fast electrons obscuring T_e measurements with electron cyclotron emission and Thomson scattering. In addition, measurements of ion temperature T_i are also difficult because of the low density of the plasma and the large shine-through effect of diagnostic neutral beam injection. On the other hand, the instability of Alfvén cascades is easily excited in such plasmas with fast ions accelerated by ion cyclotron resonance heating (ICRH), with ICRH power as low as 1 MW (in JET). Thus the ACs are always present at the early phase of discharges with ICRH and can be exploited for diagnostic purposes.

Provided that one observes the lowest frequency of ACs, $f_{\mathrm{AC}}^{\mathrm{Low}}(\mathrm{kHz}) = \omega_{\mathrm{AC}}^{\mathrm{Low}}(1/\mathrm{s})/(2\pi)$, in discharges without toroidal plasma rotation (which is small at the early phase of the discharges), and assuming that the frequency separation between the Alfvén continuum and the AC is negligibly small, $\delta\omega \ll \omega_{\mathrm{AC}}^{\mathrm{Low}}$, one obtains in accordance with Eq. (36) the following relation:

$$T_e(\mathrm{eV})\left(1+\frac{7}{4}\frac{T_i}{T_e}\right) \approx 3.77 \times [f_{\mathrm{AC}}^{\mathrm{Low}}(\mathrm{kHz})]^2. \tag{47}$$

Preliminary validation of this relation was made by using experimentally measured T_e and $f_{\mathrm{AC}}^{\mathrm{Low}}$ and assuming typical values $T_i/T_e \approx 0.5$ and $r_0/a \approx 0.33$ for a number of JET discharges. It was found that Eq. (47) holds if the ICRH power accelerating fast ions is not too high, $P_{\mathrm{ICRH}} \leqslant 3$ MW. For a higher value of ICRH power, the experimentally observed lowest AC frequency $f_{\mathrm{AC}}^{\mathrm{Low}}$ was found to be about 50% higher than that given by Eq. (47), most likely because of high values of Q_{hot} that invalidates the assumption that $\delta\omega \ll \omega_{\mathrm{AC}}^{\mathrm{Low}}$. Further experimental validation of Eq. (47) with a complete set of the necessary diagnostics is planned on JET and will be reported elsewhere.

It may also be of interest to consider a mixture of ion species when the minimum frequency of AC satisfies the generalized expression

$$\omega_{\mathrm{Geodesic}}^2 = \frac{2}{R_0^2}\frac{n_e T_e + \sum_i \gamma_i n_i T_i}{\sum_i M_i n_i}. \tag{48}$$

For the case of deuterium-tritium mixture, $M_{\mathrm{D}}=2M_{\mathrm{H}}$ and $M_{\mathrm{T}}=3M_{\mathrm{H}}$, with equal temperatures of the different ion species, $T_{\mathrm{D}}=T_{\mathrm{T}}\equiv T_i$, one obtains from (48)

$$\omega_{\mathrm{Geodesic}}^2 = \frac{2T_e}{M_{\mathrm{D}}R_0^2}\left(1+\frac{7}{4}\frac{T_i}{T_e}\right)\frac{1+n_{\mathrm{T}}/n_{\mathrm{D}}}{1+(3/2)(n_{\mathrm{T}}/n_{\mathrm{D}})}. \tag{49}$$

In this case, the relation between the minimum AC frequency and the ratio $n_{\mathrm{T}}/n_{\mathrm{D}}$ may be used for determining $n_{\mathrm{T}}/n_{\mathrm{D}}$, provided that T_e and T_i are known with sufficient accuracy.

Another interesting issue to explain, in addition to the deviation of the AC frequency at the lowest point from the shear Alfvén dispersion, is the downward frequency-sweeping ACs observed experimentally, e.g., in Fig. 2. Such

modes are very rare, and they are not described by Eq. (39). The specific condition under which these modes occur seems to be associated with a very flat $q(r)$ profile, so that a nearly zero shear region covers a significant radial width. Equation (39) has to be modified then in order to accommodate a higher-order expansion of the parallel wave number (since $d^2q/dr^2 \to 0$) and to include the spatial dependence of the fast-ion density gradient that may have a scale shorter than the magnetic shear scale. Other candidate mechanisms for the downward sweeping modes were discussed in Ref. 11. However, regardless of sweeping direction, one still expects the mode frequency of AC to track the Alfvén continuum at the zero shear point.

V. CONCLUSIONS

In this work we have extended the analytical theory of Alfvén cascades that have been observed in a variety of tokamak experiments with reversed magnetic shear. The modified theory incorporates all the essential plasma pressure effects and explains the observations that the AC spectral lines bend at low frequencies and never reach a zero-frequency point, thus deviating from the shear Alfvén wave dispersion relation. This paper establishes that the reasons for such bending are the finite pressure of the plasma and the geodesic curvature that precludes shear Alfvén perturbations from being strictly incompressible. Our analytic treatment also covers two other pressure effects on shear Alfvén waves, which are the convection in the presence of an equilibrium pressure gradient and the toroidicity-induced coupling between shear Alfvén waves and acoustic modes.

It is found that the main difference between the geodesic compressibility and the acoustic coupling is that geodesic compression does not cause a plasma displacement along the magnetic-field lines. Under this condition, the phase velocity of an AC is greater than the ion thermal velocity even in isothermal plasma, so that AC avoids a strong ion Landau damping. It was also found that the effect of plasma pressure gradient plays the role of a potential hill for ACs, not a potential well. The potential well found in Ref. 14 results from an error in sign.

This paper also suggests a plasma temperature and ion mixture diagnostics via MHD spectroscopy employing the low-frequency part of the ACs. Our preliminary attempts to explore these diagnostics are encouraging, but further dedicated experiments are needed to assess its actual capabilities.

ACKNOWLEDGMENTS

This work was supported by the U.S. Department of Energy Contract No. DE-FG03-96ER-54346. This work was funded jointly by the United Kingdom Engineering and Physical Sciences Research Counsil and by the European Communities under the contract of association between EURATOM and UKAEA. The views and opinions expressed herein do not necessarily reflect those of the European Commission. This work was carried out within the framework of the European Fusion Development Agreement.

APPENDIX: MATRIX ELEMENTS

Equation (27) can be written in form (30), where the "diagonal" operator is modified by the geodesic effect, and it has the form

$$\hat{L}_{m,m} = \frac{\partial}{\partial r}\left[(1+4\varepsilon\Delta')\frac{\omega^2}{V_A^2} - \frac{1}{R_0^2}\left(n-\frac{m}{q}\right)^2 - \frac{2C_S^2}{V_A^2R_0^2}\right] r\frac{\partial}{\partial r} - \frac{m^2}{r}\left\{[1-4\varepsilon(\varepsilon+\Delta')]\frac{\omega^2}{V_A^2} - \frac{1}{R_0^2}\left(n-\frac{m}{q}\right)^2 - \frac{2C_S^2}{V_A^2R_0^2}\right\} + o\left(\frac{1}{m}\right) + o(\varepsilon^3), \tag{A1}$$

while the "off-diagonal" operators remain similar to these derived in Ref. 4:

$$\hat{L}_{m,m\pm1} = \frac{\partial}{\partial r}\left[\frac{\omega^2}{V_A^2}(2\varepsilon+\Delta')\right] r\frac{\partial}{\partial r} + \frac{\omega^2}{V_A^2}\frac{\Delta'-\varepsilon}{r}m^2 \pm \frac{\omega^2}{V_A^2}m[\varepsilon + (r\Delta')']\frac{\partial}{\partial r} - \frac{1}{R_0^2}\left(n-\frac{m}{q}\right)\left\{\frac{\partial}{\partial r}r\Delta'\frac{\partial}{\partial r} + \frac{\Delta'+\varepsilon}{r}m^2 \pm m[\varepsilon+(r\Delta')]\frac{\partial}{\partial r}\right\}\left(n-\frac{m}{q}\right) + o\left(\frac{1}{m}\right) + o(\varepsilon^3), \tag{A2}$$

$$\hat{L}_{m\pm1,m} = \frac{\partial}{\partial r}\left[\frac{\omega^2}{V_A^2}(2\varepsilon+\Delta')\right] r\frac{\partial}{\partial r} + \frac{\omega^2}{V_A^2}\frac{\Delta'-\varepsilon}{r}m^2 \mp \frac{\omega^2}{V_A^2}m \times[\varepsilon + (r\Delta')']\frac{\partial}{\partial r} - \frac{1}{R_0^2}\left(n-\frac{m}{q}\right)\left\{\frac{\partial}{\partial r}r\Delta'\frac{\partial}{\partial r} + \frac{\Delta'+\varepsilon}{r}m^2 \mp m[\varepsilon+(r\Delta')]\frac{\partial}{\partial r}\right\}\left(n-\frac{m}{q}\right) + o\left(\frac{1}{m}\right) + o(\varepsilon^3). \tag{A3}$$

One also notes that for rational values of q, where $q=m/n$, the geodesic effect is negligibly small in expressions of the type $\hat{L}_{m\pm1,m\pm1}\Phi_{m\pm1}$, so that the contributions of the satellite harmonics in the eigenmode equation for Φ_m remain as in Ref. 4:

$$\hat{L}_{m,m-1}\{\hat{L}^{-1}_{m-1,m-1}[\hat{L}_{m-1,m}\Phi_m(r)]\} + \hat{L}_{m,m+1}\{\hat{L}^{-1}_{m+1,m+1}[\hat{L}_{m+1,m}\Phi_m(r)]\} = 2r\frac{\omega^2}{V_A^2}\left\{\frac{\partial^2}{\partial r^2}\left[\frac{(\Delta'+\varepsilon)^2}{(2qn-2m)^2-1} + \varepsilon(2\Delta'+\varepsilon)\right] - \left(\frac{m}{r}\right)^2\left[\frac{(\Delta')^2}{(2qn-2m)^2-1} - \varepsilon(2\Delta'+\varepsilon)\right]\right\}\Phi_m. \tag{A4}$$

Combining Eqs. (A1) and (A4) gives the eigenmode equation (31).

The effect of the thermal plasma pressure gradient modifies the expressions for the matrix elements [Eqs. (A1)–(A3)] as follows:

$$\hat{L}_{m,m\pm1}^{\text{pressure}} = \hat{L}_{m,m\pm1} \mp \frac{\alpha}{2}\frac{m}{q_0^2 R_0^2}\frac{\partial}{\partial r} - \frac{\alpha}{2}\frac{m^2}{r q_0^2 R_0^2}. \tag{A5}$$

Following the procedure described in Ref. 4 and neglecting the cross-product terms of the type $\alpha\Omega^2(\varepsilon_0-\Delta')$, which are $o(\varepsilon^2)$ in comparison with α^2 for $\Omega^2<1/4$, one obtains Eq. (45).

[1] S. E. Sharapov, D. Testa, B. Alper, D. N. Borba, A. Fasoli, N. C. Hawkes, R. F. Heeter, M. J. Mantsinen, and M. von Hellermann, Phys. Lett. A **289**, 127 (2001).

[2] H. L. Berk, D. N. Borba, B. N. Breizman, S. D. Pinches, and S. E. Sharapov, Phys. Rev. Lett. **87**, 185002 (2001).

[3] S. E. Sharapov, B. Alper, H. L. Berk, D. N. Borba, B. N. Breizman, C. D. Challis, A. Fasoli, N. C. Hawkes, T. C. Hender, J. Mailloux, S. D. Pinches, D. Testa, and contributors to the EFDA-JET work programme, Phys. Plasmas **9**, 2027 (2002).

[4] B. N. Breizman, H. L. Berk, M. S. Pekker, S. D. Pinches, and S. E. Sharapov, Phys. Plasmas **10**, 3649 (2003).

[5] H. Kimura, Y. Kusama, M. Saigusa, G. J. Kramer, K. Tobita, M. Nemoto, T. Kondoh, T. Nishitani, O. Da Costa, T. Ozeki, T. Oikawa, S. Moriyama, A. Morioka, G. Y. Fu, C. Z. Cheng, and V. I. Afanas'ev, Nucl. Fusion **38**, 1303 (1998).

[6] J. A. Snipes, N. Basse, C. Boswell, E. Edlund, A. Fasoli, N. N. Gorelenkov, R. S. Granetz, L. Lin, Y. Lin, R. Parker, M. Porkolab, J. Sears, S. E. Sharapov, V. Tang, and S. Wukitch, Phys. Plasmas **12**, 056102 (2005).

[7] R. Nazikian, G. J. Kramer, C. Z. Cheng, N. N. Gorelenkov, H. L. Berk, and S. E. Sharapov, Phys. Rev. Lett. **91**, 125003 (2003).

[8] R. Nazikian, B. Alper, H. L. Berk, D. Borba, C. Boswell, R. V. Budny, K. H. Burrell, C. Z. Cheng, E. J. Doyle, E. Edlund, R. J. Fonck, A. Fukuyama, N. N. Gorelenkov, C. M. Greenfield, D. J. Gupta, M. Ishikawa, R. J. Jayakumar, G. J. Kramer, Y. Kusama, R. J. La Haye, G. R. McKee, W. A. Peebles, S. D. Pinches, M. Porkolab, J. Rapp, T. L. Rhodes, S. E. Sharapov, K. Shinohara, J. A. Snipes, W. M. Solomon, E. J. Strait, M. Takechi, M. A. Van Zeeland, W. P. West, K. L. Wong, S. Wukitch, and L. Zeng, *Fusion Energy 2004*, Proceedings of the 20th International Conference on Fusion Energy, Vilamoura, 2004 (IAEA, Vienna, 2004), Paper EX/5-1 (http://www-naweb.iaea.org/napc/physics/fec/fec2004/datasets/index.html).

[9] E. Joffrin, C. D. Challis, G. D. Conway, X. Garbet, A. Gude, S. Gunter, N. C. Hawkes, T. C. Hender, D. F. Howell, G. T. A. Huysmans, E. Lazzaro, P. Maget, M. Marachek, A. G. Peeters, S. D. Pinches, S. E. Sharapov, and JET-EFDA contributors, Nucl. Fusion **43**, 1167 (2003).

[10] S. E. Sharapov, B. Alper, J. Fessey, N. C. Hawkes, N. P. Young, R. Nazikian, G. J. Kramer, D. N. Borba, S. Hacquin, E. De La Luna, S. D. Pinches, J. Rapp, D. Testa, and JET-EFDA contributors, Phys. Rev. Lett. **93**, 165001 (2004).

[11] F. Zonca, S. Briguglio, L. Chen, S. Dettrick, G. Fogaccia, D. Testa, and G. Vlad, Phys. Plasmas **9**, 4939 (2002).

[12] N. Winsor, J. L. Johnson, and J. M. Dawson, Phys. Fluids **11**, 2448 (1968).

[13] M. S. Chu, J. M. Greene, L. L. Lao, A. D. Turnbull, and M. S. Chance, Phys. Fluids B **4**, 3713 (1992).

[14] G. J. Kramer, N. N. Gorelenkov, R. Nazikian, and C. Z. Cheng, Plasma Phys. Controlled Fusion **46**, L23 (2004).

[15] V. A. Mazur and A. B. Mikhailovskii, Nucl. Fusion **17**, 193 (1977).

[16] F. Zonca, L. Chen, and R. Santoro, Plasma Phys. Controlled Fusion **38**, 2011 (1996).

[17] B. B. Kadomtsev, *Hydromagnetic Stability of a Plasma*, in Reviews of Plasma Physics, Vol. 2, edited by M. A. Leontovich (Consultants Bureau, New York, 1966), p. 155.

[18] S. E. Sharapov, A. B. Mikhailovskii, and G. T. A. Huysmans, Phys. Plasmas **11**, 2286 (2004).